THERMAL NEUTRON DEMAGNETIZATION OF NdFeB MAGNETS

R. Klaffky, USDOE, Germantown, MD 20874, U.S.A

R. Lindstrom, B. Maranville, R. Shull, NIST, Gaithersburg, MD 20899, U.S.A

B. J. Micklich , J. Vacca, ANL, Argonne, IL 60439, U.S.A.

.

Abstract

To isolate the effect that thermal neutrons have on $Nd_2Fe_{14}B$ permanent magnets, the magnetization and coercivity were studied as a function of dose. The changes in remanent magnetization are substantial and are attributed to boron thermal neutron capture through the $^{10}B(n,alpha)^7Li$ reaction, which generates MeV energy alpha particles and lithium ions. MCNPX Monte Carlo calculations were used to simulate energy deposition in the APS Sector 3 insertion device magnets and the predicted gamma and neutron fluxes are compared to Au and Ti foil dosimetry. These calculations indicate that high linear energy transfer (LET) alpha particles coming from fast neutron (10 keV to 10 MeV) reactions with the boron and with materials close to the magnets (aluminum and vanadium permendur) are primarily responsible for the demagnetization. There will also be Li ion contributions in connection with the boron reactions. The MCNPX calculations predict that the thermal neutron fluxes are low, which is confirmed by Au foil dosimetry.

INTRODUCTION

At accelerator facilities $Nd_2Fe_{14}B$ magnets have enjoyed wide use because of desirable properties such as high remanent fields and low cost. However, when these magnets are located in high radiation areas they can lose magnetization with a degradation in performance. At the Advanced Photon Source (APS) at Argonne National Laboratory, $Nd_2Fe_{14}B$ insertion devices have shown losses of magnetization on a few straight sections where the largest electron beam losses occur due to limiting vacuum chamber apertures. In the worst case, these magnetization losses were evident after a three month operational period. There have been other studies of the effect of fast neutron irradiations of $Nd_2Fe_{14}B$ magnets [1,2,3] and for thermal neutrons at low doses [2]. In this study the effect of thermal neutron doses on the magnetization and coercivity of two $Nd_2Fe_{14}B$ grades was measured for doses ranging from 4.9×10^{12} to 8.9×10^{13} neutrons/cm^2. To study the demagnetization process in APS undulators, the Monte Carlo code MCNPX [4] was used to model the energy deposited in the insertion device magnets.

NEUTRON IRRADIATIONS

Neutron irradiations were performed at the NIST Center for Neutron Research (NCNR). All samples were 3.16 mm diameter discs. The N45 and N48 grade samples purchsed from K&J Magnetics were 0.80 and 1.59 mm thick, respectively. The manufacturer specifies residual flux densities B_r, (BH)max, and Curie temperature values of 13.3-13.7kG, 43-45 MGOe, 583 K for the N45 grade and 13.8-14.2kG, 46-48MGOe, 583 K for the N48 grade. The thermal column rabbit facility was used, where the thermal neutron flux is $3x10^{11}$ n/cm^2-sec. The epithermal and fast (fission spectrum) fluxes are lower by factors of 5×10^3 and 8×10^5 respectively. Because boron is an efficient neutron absorber, the mean flux experienced throughout the samples was about 70 per cent of the flux measured by gold foil dosimeters [5].

MAGNETIC MEASUREMENTS

The remanent moment M_{rem} (M at H=0) before and after neutron irradiation was measured with a SQUID magnetometer at room temperature. In Figure 1, we see a hysteresis loop of sample DB3561 (N48 grade) before and after irradiation. A reduced initial magnetization (M_{rem}) is apparent for the irradiated sample, while the full saturation magnetization is recovered when the field is increased to 5 Tesla. There is no change in coercivity with neutron irradiation.

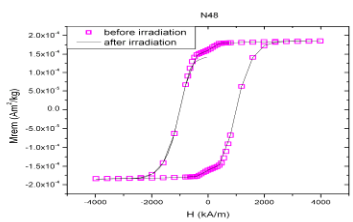

Fig. 1: Hysteresis of N48 neutron-irradiated sample

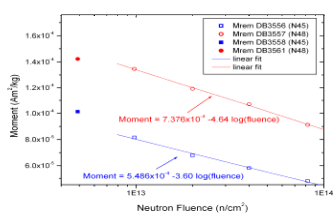

Fig. 2: Remanent Moment Neutron Dose Dependence

The remanent moment decreases with the logarithm of the dose (Fig.2), indicating a trend towards saturation at high doses. At 8.9 x10 ^{12} n/cm^2 there is a large initial 43 % decrease in the DB3556 (N45 grade) sample which we attribute to demagnetization from heating of the samples during the first neutron irradiation. The heating is predominantly from the ^{10}B(n,alpha)^{7}Li reaction which will cause the same heating in all of the samples since they have the same 1% boron concentration. Temperature scans were performed to confirm the temperature sensitivity of the N45 samples. The N48 sample showed no temperature dependence up to 360 K while the N45 sample shows changes after being heated to 350 K. We therefore estimate that the sample irradiation temperature was less than 350 K.

THERMAL SPIKE MODEL

The dominant effect of the thermal neutron irradiation comes from the ^{10}B(n,α)^{7}Li capture reaction on the 19.8% isotope, with a cross section of 3837b. Most of the energy released in this reaction (2789 keV) is shared between the alpha particle (1.45 MeV) and the recoil lithium nucleus (0.85 MeV). The kinetic energy shared by the helium and lithium nuclei is lost predominantly by interaction with lattice electrons, over mean distances of 2.7 µm and 1.4 µm respectively [6]. This results in high LET values of 0.54 keV/nm and 0.61 keV/ nm which can be treated by the thermal spike model [7]. Initial electron temperatures can exceed 1,000 K, even reaching temperatures approaching 10,000 K [8]. There will be a large local lattice temperature increase in the spike region that extends over several micron-sized $Nd_2Fe_{14}B$ grains. The lattice temperature in this region can approach or exceed the Curie temperature (593-613K), leading to nucleation of reversely magnetized grains. It should be noted that, in comparison, 1 MeV protons and electrons have ranges of 7 and 800 µm respectively, with much lower LET values of 0.14 keV/nm and .0013 keV/nm.

MCNPX SIMULATIONS OF ENERGY DEPOSITION IN APS MAGNETS

We used version 2.5.0 of the Monte Carlo code MCNPX [4] to help determine the important demagnetization mechanisms. MCNPX is capable of transporting neutrons and light ions as well as electrons and photons, and thus can provide an indication as to the extent that these particles contribute to the demagnetization. The geometry is shown in Figure 3. We included the copper vacuum transition boxes at each end, because they can contribute significantly to gamma and neutron production. The beam loss scenario assumes that 10^8 electrons/second are lost along the vacuum chamber length at the tip of the inboard major radius (at the right edge of the vacuum chamber in Figure 3 (a) at an angle of 500 microradians). Some of these electrons (about 16%) strike the copper transition box just at the entrance to the ID vacuum chamber, creating neutrons that travel into the magnet region. The magnets are $Nd_2Fe_{14}B$ and the pole pieces vanadium permendur.

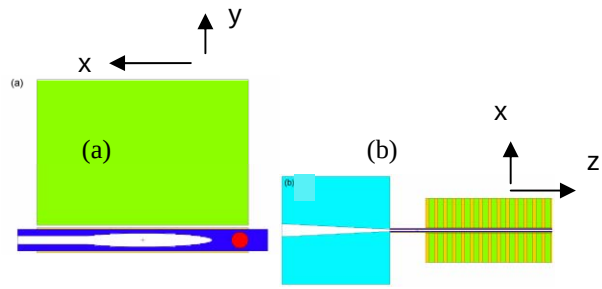

Fig. 3: (a) x-y cut of vacuum chamber and upper magnet.
(b) z-y profile of the upstream end of the vacuum chamber.

In this figure, x is radially outward from the ring, y is vertical, and z is along the electron path. The dominant energy deposition is due to electrons and photons, as has been reported in an earlier Monte Carlo simulation [9]. There is a much smaller energy deposition due to neutrons and light ions. Of the latter contribution, about 3.5% is due to products of the reaction ^{10}B(n,alpha)^{7}Li. Tally results show that 84-88% of the energy deposited in this reaction is due to neutrons with incident energies of 10 keV to 10 MeV. The energy deposited in the magnets as a function of axial position is shown in Figure 4.

The radiation dose in the 5mm of the magnet closest to the ID vacuum chamber is about 7-8 times the average dose. For neutrons and light ions, the dose is about 2.5 times the average. Inclusion of a 0.60 mm lead shield immediately outside the vacuum chamber reduces the dose to the magnets by about 20 per cent.

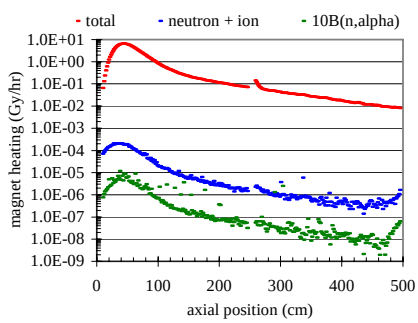

Fig. 4: Axial heating profile showing the dose rate in the first 5 mm of the magnet.

An important feature to note is that previous magnetic measurements on the Sector 3 APS undulators have shown that the upstream undulator (at 0-240 cm) has exhibited the most pronounced demagnetization on its upstream side, and the downstream undulator (at 260-500 cm) the most pronounced demagnetization on the

downstream side [10]. This correlates very well with the neutron and ion energy deposition curves which not only show an upstream maximum, but also an increase at the downstream ID section due to the production of neutrons from electrons and gammas striking the downstream copper transition. The neutrons then generate high LET ions in the magnets and in the materials surrounding the magnets (aluminum, vanadium permendur). As we have seen from the thermal neutron irradiation of $Nd_2Fe_{14}B$, it is these ions that are very effective in demagnetizing the magnets. The increase can not be explained by the gamma and electron heating which monotonically decrease along the undulator axis.

Total energy deposition is highest where the electron beam hits the vacuum chamber wall. Energy deposition in the magnet is localized around the point nearest the beam strike. Most of the energy is deposited in the form of ionization by electrons. Direct energy deposition by photons and neutrons is relatively low. However, most energy deposition due to photoneutrons created in the shower is actually deposited by light ions such as protons and alphas. Proton heating occurs primarily in the magnet, while alpha heating peaks in the vacuum chamber wall, with a smaller amount in the magnet which is comparable to the proton heating. The high LET alpha particles are expected to be primarily responsible for the demagnetization and could explain the limited depth range of the demagnetization previously reported [9]. The calculated photon and fast neutron fluxes are shown in Figure 5.

PHOTON AND NEUTRON DOSIMETRY

Samples of pure Au and Ti sheet were placed inside the ID 4 undulator during each of two successive 144-hour runs of the accelerator, and then the induced radioactivity was assayed by gamma counting at NIST. Radioisotopes

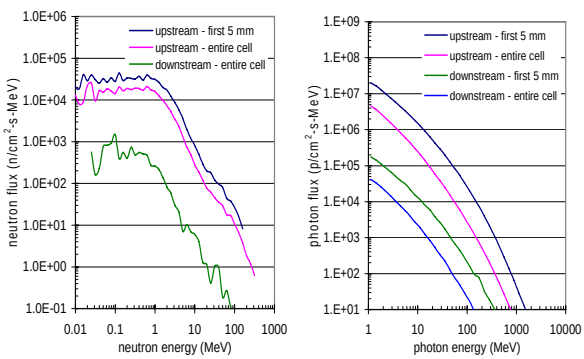

Fig. 5: Neutron and photon fluxes per Mev

of gold and scandium were measured. The thermal neutron-capture product ^{198}Au was found to be much less than ^{196}Au. The latter can be produced from stable ^{197}Au by either of two reactions: (γ, n) (threshold 8.1 MeV) or (fast n, 2n) (threshold 8.1 MeV). Fast (MeV) neutrons on titanium produce ^{46}Sc, ^{47}Sc, and ^{48}Sc by (n,p) reactions with thresholds of 1.6 MeV, 0, and 3.2 MeV, respectively, but these products can also be produced by (γ,p) reactions, with thresholds all about 11 MeV. Because the activity per target atom of ^{47}Sc was measured to be much greater than the other isotopes, the radioactivity can be ascribed predominantly to fast neutrons.

The Au foils indicated thermal neutron fluxes of only 42 to 135 n/cm^2-s. The thermal neutron flux is low, as expected, and the foil-determined γ flux of 6000-8000 γ/cm^2-s compares favorably with the MCNPX value of 5500 obtained by multiplying the MCNPX downstream entire cell value of 1,100/cm^2-s-Mev at 13 MeV times the 5 MeV FWHM of the sharp 13 MeV Au (γ,n) reaction. The Ti foil-determined neutron flux of $8x10^5$/cm^2-s utilizes average Ti fission flux cross sections over 1-20 MeV for the Ti (n,p) reactions. After multiplying the MCNPX values in Figure 5 by 20 MeV, we obtain approximately a $2x10^5$/ cm^2-s fast neutron flux for the first 5 mm of the upstream ID magnet. This is in better agreement with the foil measurement than the downstream MCNPX value.

ACKNOWLEDGEMENTS

R. Klaffky expresses his appreciation for helpful discussions with John Grimmer, Liz Moog, Mohan Ramanathan, Brian Rusthoven, Sushil Sharma, Isaac Vasserman, and C-Y. Yao of the Advanced Photon Source at ANL.

REFERENCES

[1] R. D. Brown and J .R. Cost, "Radiation-Induced Changes in Magnetic Properties of Nd-Fe-B Permanent Magnets", IEEE Trans. Mag 25(1989) 3117-3120.
[2] J. Alderman, P. K. Job, R. C. Martin, C. M. Simmons, and G. D. Owen, Nucl. Instr. And and Meth. A 481 (2002) 9.
[3] S.Anderson, J. Spencer, Z. Wolf, A. Baldwin, D. Pellet, M. Boussoufi, and J. Volk, "Fast Neutron Damage Studies on NdFeB Materials", PAC'05, Knoxville, May 2005.
[4] D. Pelowitz, ed., "MCNPX User's Manual, Version 2.5.0," LA-CP-05-0369 (April 2005).
[5] R. F. Fleming, "Neutron Self-shielding Factors for Simple Geometries", Int. J. Appl. Rad. Isot. 33 (1982), 1263-1268.
[6] J. Ziegler, SRIM - The Stopping and Range of Ions in Matter (www.srim.org)
[7] F. Seitz and J. F. Koehler, Solid State Phys. 2 (1956) 305.
[8] M. Caron, H. Rothard, M. Toulemonde, B. Gervais, M. Beuve, Nucl. Instr. and Meth. B 245 , 36 (2006).
[9] Shigemi Sasaki, Maria Petra, Isaac B. Vasserman, Charles L. Doose, Elizabeth R. Moog, N. V. Mokhov, PAC'05, Knoxville, May 2005.
[10] Experimental Facilities Division/User Program Division Technical Progress Reports (ANL/APS/TB-47, 2002) and (ANL/APS/TB-38, 2000).